Design of a native-like secreted form of the hepatitis C virus E1E2 heterodimer

Johnathan D. Guest[a,b], Ruixue Wang[a], Khadija H. Elkholy[a,c], Andrezza Chagas[a], Kinlin L. Chao[a,b], Thomas E. Cleveland IV[a,d], Young Chang Kim[e], Zhen-Yong Keck[e], Alexander Marin[a], Abdul S. Yunus[a], Roy A. Mariuzza[a,b], Alexander K. Andrianov[a], Eric A. Toth[a], Steven K. H. Foung[e], Brian G. Pierce[a,b,1], and Thomas R. Fuerst[a,b,1]

[a]Institute for Bioscience and Biotechnology Research, University of Maryland, Rockville, MD 20850; [b]Department of Cell Biology and Molecular Genetics, University of Maryland, College Park, MD 20742; [c]Molecular Biology Department, Genetic Engineering and Biotechnology Division, National Research Centre, Cairo 12622, Egypt; [d]Biomolecular Measurement Division, National Institute of Standards and Technology, Gaithersburg, MD 20899; and [e]Department of Pathology, Stanford University School of Medicine, Stanford, CA 94305

Edited by Peter Palese, Icahn School of Medicine at Mount Sinai, New York, NY, and approved November 27, 2020 (received for review July 17, 2020)

Hepatitis C virus (HCV) is a major worldwide health burden, and a preventive vaccine is needed for global control or eradication of this virus. A substantial hurdle to an effective HCV vaccine is the high variability of the virus, leading to immune escape. The E1E2 glycoprotein complex contains conserved epitopes and elicits neutralizing antibody responses, making it a primary target for HCV vaccine development. However, the E1E2 transmembrane domains that are critical for native assembly make it challenging to produce this complex in a homogenous soluble form that is reflective of its state on the viral envelope. To enable rational design of an E1E2 vaccine, as well as structural characterization efforts, we have designed a soluble, secreted form of E1E2 (sE1E2). As with soluble glycoprotein designs for other viruses, it incorporates a scaffold to enforce assembly in the absence of the transmembrane domains, along with a furin cleavage site to permit native-like heterodimerization. This sE1E2 was found to assemble into a form closer to its expected size than full-length E1E2. Preservation of native structural elements was confirmed by high-affinity binding to a panel of conformationally specific monoclonal antibodies, including two neutralizing antibodies specific to native E1E2 and to its primary receptor, CD81. Finally, sE1E2 was found to elicit robust neutralizing antibodies in vivo. This designed sE1E2 can both provide insights into the determinants of native E1E2 assembly and serve as a platform for production of E1E2 for future structural and vaccine studies, enabling rational optimization of an E1E2-based antigen.

hepatitis C virus | envelope glycoprotein | vaccine | E1E2 | scaffold

Hepatitis C virus (HCV) is a global disease burden, with an estimated 71 million people infected worldwide (1, 2). Roughly 75% of HCV infections become chronic (3–5) and in severe cases can result in cirrhosis or hepatocellular carcinoma (6). Viral infection can be cured at high rates by direct-acting antivirals, but multiple public health and financial barriers (7, 8), along with the possibility of reinfection or continued disease progression (7, 9, 10), have resulted in a continued rise in HCV infections. An HCV vaccine remains essential to proactively protect against viral spread, yet vaccine developments against the virus have been unsuccessful to date (11, 12). The challenges posed by HCV sequence diversity (12, 13), glycan shielding (14, 15), immunodominant nonneutralizing epitopes (16–19), and preparation of a homogeneous E1E2 antigen all contribute to the difficulty in generating protective B cell immune responses. Although multiple studies in chimpanzees and humans have used E1E2 formulations to induce a humoral immune response, their success in generating high titers of broadly neutralizing antibody (bnAb) responses has been limited (20). Optimization of E1E2 to improve its immunogenicity and elicitation of bnAbs through rational design may lead to an effective B cell-based vaccine (21).

HCV envelope glycoproteins E1 and E2 form a heterodimer on the surface of the virion (22–24). Furthermore, E1E2 assembly has been proposed to form a trimer of heterodimers (25) mediated by hydrophobic C-terminal transmembrane domains (TMDs) (24, 26, 27) and interactions between E1 and E2 ectodomains (28–30). These glycoproteins are necessary for viral entry and infection, as E2 attaches to the CD81 and SR-B1 coreceptors as part of a multistep entry process on the surface of hepatocytes (31–34). Neutralizing antibody responses to HCV infection target epitopes in E1, E2, or the E1E2 heterodimer (18, 35–40). Structural knowledge of bnAb antibody–antigen interactions, which often target E2 epitopes in distinct antigenic domains B, D, or E (18, 41, 42), can inform vaccine design efforts to induce bnAb responses against flexible HCV epitopes (43–45). E1E2 bnAbs, including AR4A, AR5A (46), and others recently identified (38), are not only among the most broadly neutralizing (35) but also represent E1E2 quaternary epitopes unique to antibody recognition of HCV.

Although much is known about bnAb responses to E1E2 glycoproteins, induction of B cell-based immunity with an E1E2-based

Significance

Hepatitis C virus infects 1% of the world's population, with no vaccine currently available. One vaccine candidate is the membrane-associated E1E2 envelope glycoprotein which has been used in clinical studies. However, a major challenge to both structural studies and rational vaccine design is high-yield production of homogenous E1E2. Production of E1E2 liberated from the membrane with native structure and antigenicity would thus represent a major advance. We describe the design and validation of a soluble, secreted E1E2 (sE1E2) antigen in which a scaffold replaces its transmembrane domains and enforces assembly. High-affinity sE1E2 binding to broadly neutralizing antibodies and to its receptor CD81, along with robust immunogenicity, makes this a promising platform for high-resolution structural characterization and vaccine development.

Author contributions: J.D.G., R.W., K.H.E., A.C., T.E.C., Y.C.K., Z.-Y.K., A.M., A.S.Y., R.A.M., A.K.A., E.A.T., S.K.H.F., B.G.P., and T.R.F. designed research; J.D.G., R.W., K.H.E., A.C., K.L.C., T.E.C., Y.C.K., Z.-Y.K., A.M., A.S.Y., R.A.M., A.K.A., and E.A.T. performed research; J.D.G., R.W., K.H.E., A.C., K.L.C., Z.-Y.K., A.M., R.A.M., A.K.A., E.A.T., S.K.H.F., B.G.P., and T.R.F. analyzed data; and J.D.G., E.A.T., B.G.P., and T.R.F. wrote the paper.

The authors declare no competing interest.

This article is a PNAS Direct Submission.

[1]To whom correspondence may be addressed. Email: pierce@umd.edu or tfuerst@umd.edu.

This article contains supporting information online at https://www.pnas.org/lookup/suppl/doi:10.1073/pnas.2015149118/-/DCSupplemental.

Published January 11, 2021.

vaccine immunogen (47–49) has remained difficult. The inherent hydrophobicity of E1 and E2 TMDs (24, 50) may impede uniform production of an immunogenic E1E2 heterodimer that could be utilized for both vaccine development and E1E2 structural studies. Although partial E1 and E2 structures have been determined (39, 51–54), many other enveloped viruses have structures of a complete and near-native glycoprotein assembly (55–59), providing a basis for rational vaccine design (60–62). Viral glycoproteins of influenza hemagglutinin (63), respiratory syncytial virus (RSV) (55), severe acute respiratory syndrome coronavirus 2 (64), and others (65, 66) have been stabilized in soluble form using a C-terminal attached foldon trimerization domain to facilitate assembly. HIV gp120–gp41 proteins have been designed as soluble SOSIP trimers in part by introducing a furin cleavage site to facilitate native-like assembly when cleaved by the enzyme (56, 67). Previously described E1E2 glycoprotein designs include covalently linked E1 and E2 ectodomains (68, 69), E1E2 with TMDs intact and an immunoglobulin G (IgG) Fc tag for purification (70), as well as E1 and E2 ectodomains with a cleavage site (68), which presented challenges for purification either due to intracellular expression or to high heterogeneity. Two recently described scaffolded E1E2 designs, while promising, have not been shown to engage monoclonal antibodies (mAbs) that recognize the native E1E2 assembly, though they were engaged by E1-specific and E2-specific mAbs, as well as coreceptors that recognize E2 (71). Therefore, these presentations of E1E2 glycoproteins may not represent a native and immunogenic heterodimeric assembly, and thus their potential as vaccine candidates remains unclear.

Here, we describe the design of a secreted E1E2 glycoprotein (sE1E2) that mimics both the antigenicity in vitro and the immunogenicity in vivo of the native heterodimer through the scaffolding of E1E2 ectodomains. In testing our designs, we found that both replacing E1E2 TMDs with a leucine zipper scaffold and inserting a furin cleavage site between E1 and E2 enabled secretion and native-like sE1E2 assembly. We assessed the size, heterogeneity, antigenicity, and immunogenicity of this construct (identified as sE1E2.LZ) in comparison with full-length membrane-bound E1E2 (mbE1E2). sE1E2.LZ binds a broad panel of bnAbs to E2 and E1E2, as well as coreceptor CD81, providing evidence of assembly into a native-like heterodimer. An immunogenicity study indicated that sera of mice injected with sE1E2.LZ neutralize HCV pseudoparticles at levels comparable to sera from mice immunized with mbE1E2. This sE1E2 design is a form of the native E1E2 heterodimer that both improves upon current designs and represents a platform for structural characterization and engineering of additional HCV vaccine candidates.

Results

Design of sE1E2 Constructs. We designed and screened a set of sE1E2 constructs to determine which type of scaffold might be suitable for development of a native-like secreted heterodimer (Fig. 1*A*). Scaffolded sE1E2 constructs were synthesized as cleavable polyproteins and contain a six-arginine furin cleavage site, which was incorporated to facilitate E1E2 assembly similar to HIV SOSIP constructs (56). Each cleavable polyprotein replaces E1 and E2 TMDs with a self-assembling heterodimeric, homotrimeric, or heterohexameric scaffold designed to enforce E1E2 ectodomain assembly in the absence of a membrane anchor. In addition, all constructs replace the N-terminal wild-type signal peptide sequence with a modified version of the signal sequence from tissue plasminogen activator (tPA) (72) and include a C-terminal 6xHis tag for purification.

sE1E2.LZ used the human c-Fos/c-Jun leucine zipper, a coiled-coil obligate heterodimer with a known structure (Protein Data Bank [PDB] ID code 1FOS; Fig. 1*B*) (73), as a scaffold. The heterodimeric c-Fos/c-Jun leucine zipper has been used as a scaffold for expression of T cell receptors (74), making it a possible candidate for maintaining heterodimeric E1E2 in secreted form. sE1E2.FD replaced the E1 TMD with a foldon domain (PDB ID code 4NCU; Fig. 1*C*) (75), a self-trimerizing protein that has been previously used to stabilize soluble assemblies of viral glycoprotein trimers (55, 76). This construct was designed to test whether enforcing E1 trimerization (25) would be sufficient to enable E1E2 ectodomain assembly. sE1E2.CC used a scaffold that was designed to self-assemble into a heterohexameric peptide complex, which would reflect the previously described model of the E1E2 TMD architecture (25) in a soluble form. The corresponding scaffold, CC1+CC2 (Fig. 1*D*), was designed de novo using the HBNet protocol of Rosetta protein modeling software (77) (*SI Appendix*, *Supplementary Information Text*). Though we were unable to confirm the structure of CC1+CC2 with experimental structural determination, it was included as a candidate scaffold given its putative hexameric assembly (*SI Appendix*, Fig. S1). To examine the importance of including scaffolds in the absence of TMDs, a separate construct with a furin cleavage site but no scaffold was generated (sE1E2.R6). Two sE1E2 constructs with a covalent linker between ectodomains were also included. In sE1E2GS3, E1 and E2 ectodomains are linked by a 15-amino-acid glycine–serine sequence, similar to a previously described sE1E2 construct (68). The construct sE1E2RevGS3 reverses the order of E1 and E2 ectodomains, testing whether altering the order of ectodomains in the context of a covalent fusion may improve E1E2 assembly, which could be affected by the currently unknown proximity of the N and C termini of the ectodomains in native E1E2.

sE1E2.LZ Forms an Intact E1E2 Complex. Each sE1E2 construct was expressed in mammalian cells, with cleavable polyproteins coexpressed with furin. To test for successful secretion of sE1E2, we probed for the presence of E1 and E2 ectodomains in the supernatant, using the E1 human mAb (HMAb) H-111 (78) and the E2 HMAb HCV1 (79) in Western blots. These antibodies bind to linear epitopes at or near the N terminus of the E1 or E2 ectodomain, respectively. sE1E2.LZ was the only cleavable polyprotein design to show clear detection of both E1 and E2 in the supernatant (Fig. 2), though sE1E2.FD exhibited some secretion of E2. The scaffoldless sE1E2.R6 construct showed no secretion of sE1E2, consistent with previous results that E1 and E2 ectodomains alone do not form a stable complex (71). Expression of E1-Jun and E2-Fos constructs *in trans* without a furin cleavage site found secretion of E1-Jun but minimal secretion of E2-Fos (*SI Appendix*, Fig. S2). Collectively, these results determine that the combination of a furin cleavage site and leucine zipper scaffold enables secretion of the E1E2 complex. sE1E2GS3 and sE1E2RevGS3 showed high levels of E1 and E2 in supernatant, corroborating previous findings with a covalently linked sE1E2 design that is similar to sE1E2GS3, which was likewise detected in the supernatant (68). In addition, we examined if protein was expressed but not secreted by probing for the presence of E1 and E2 in lysed cells (*SI Appendix*, Fig. S3). sE1E2GS3 and sE1E2RevGS3 that was retained in cells migrated at smaller molecular weights than the corresponding secreted proteins, while sE1E2.FD and sE1E2.LZ exhibited multiple bands in E2 detection; both results may be indicative of incomplete processing or degradation of unsecreted protein. Though some sE1E2.LZ was detected intracellularly, ~90% of expressed sE1E2.LZ was secreted to the supernatant, as determined by a quantitative analysis comparing supernatant and cell lysate Western blots probed with the anti-E2 HMAb HCV1 (*SI Appendix*, Fig. S4). Based on these results, we selected sE1E2.LZ, as a cleaved scaffolded sE1E2 candidate, and sE1E2GS3, as a covalently linked sE1E2 candidate, for further characterization.

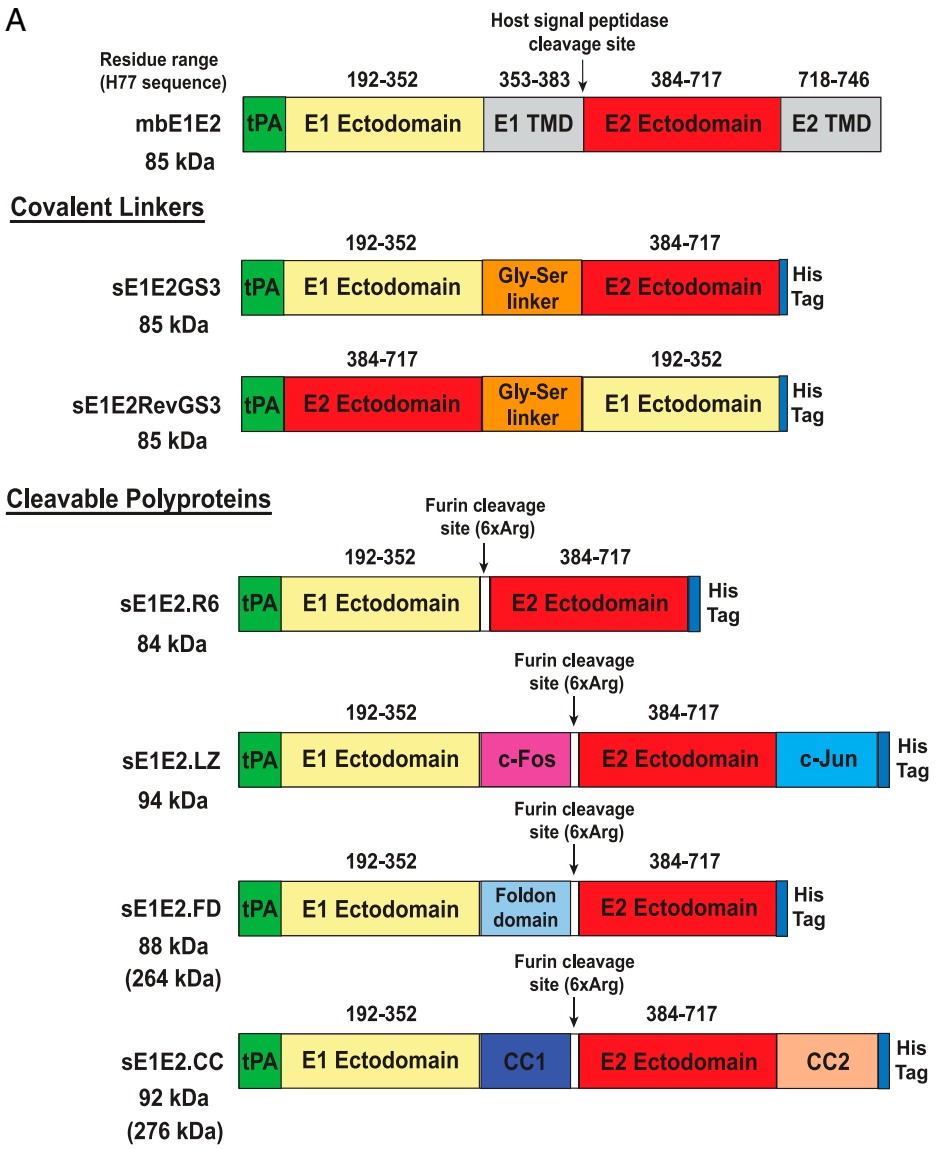

Fig. 1. Design of sE1E2 constructs. (*A*) Schematic of mbE1E2, covalent linker sE1E2 constructs, and cleavable polyprotein constructs. Regions shown include tPA signal sequence (green box), E1 ectodomain (yellow boxes), E2 ectodomain (red boxes), wild-type TMDs (gray boxes), Gly-Ser linker (orange boxes), and various scaffolds replacing TMDs. E1E2 residue ranges for each region are noted according to H77 numbering. C-terminal His tags and furin cleavage sites are shown in boxes and labeled. The expected molecular weight of each construct is indicated, and molecular weights of expected oligomers for sE1E2.FD and sE1E2.CC are in parentheses. For molecular weight estimations, each N-glycan is approximated to be 2 kDa at each NxS/NxT sequon, a value within the molecular weight range of typical N-linked glycans (108). (*B*) X-ray structure of human c-Fos/c-Jun heterodimer (PDB ID code 1FOS); only the coiled-coil region that was used for the sE1E2.LZ scaffold is shown. c-Fos and c-Jun chains were colored to match the diagram of sE1E2.LZ. (*C*) X-ray structure of foldon domain (PDB ID code 4NCU). All chains are colored light blue to match the diagram for sE1E2.FD. (*D*) Model of CC1+CC2 heterohexameric peptide assembly. CC1 and CC2 chains are colored to match the diagram for sE1E2.CC. All structures were visualized in PyMOL (Schrodinger, LLC).

Purification of sE1E2.LZ. We purified both sE1E2.LZ and sE1E2GS3 using immobilized metal affinity chromatography (IMAC) and then examined the molecular weight and heterogeneity of each construct with size-exclusion chromatography (SEC) (Fig. 3*A* and *SI Appendix*, Fig. S5). Expression and purification of these constructs produced sufficiently pure protein for characterization, with sE1E2.LZ providing the highest yield at 480 μg/100 mL of transfected cells (*SI Appendix*, Fig. S6). sE1E2.LZ and sE1E2GS3 eluted from the Superdex 200 column across a broad molecular weight range, with the peak for each estimated at ∼400 kDa. The resultant SEC peaks were directly compared with the peak SEC fractions of purified mbE1E2 (Fig. 3*D*). Although sE1E2.LZ, along with sE1E2GS3, exhibited a broad peak in SEC, it eluted at a volume consistent with a molecular weight that is both smaller than mbE1E2, which eluted as a peak in void volume (∼700 kDa), and closer to the expected size of the heterodimeric assembly (94 kDa; Fig. 1). To further investigate the size distribution and heterogeneity of purified constructs, we examined fractions eluted from SEC under nonreducing conditions, using Western blot for sE1E2.LZ (Fig. 3 *B* and *C*), mbE1E2 (Fig. 3 *E* and *F*), and sE1E2GS3 (*SI Appendix*, Fig. S7 *D* and *F*), and sodium dodecyl sulfate polyacrylamide gel electrophoresis (SDS/PAGE) for sE1E2GS3 (*SI Appendix*, Fig. S7*B*) and sE1E2.LZ (*SI Appendix*, Fig. S8*B*). Both sE1E2.LZ and sE1E2GS3 SEC fractions showed two predominant species migrating in the range between 150 and 250 kDa when probed for E1 and E2 under nonreducing conditions, which is smaller than expected based on the SEC chromatographs but

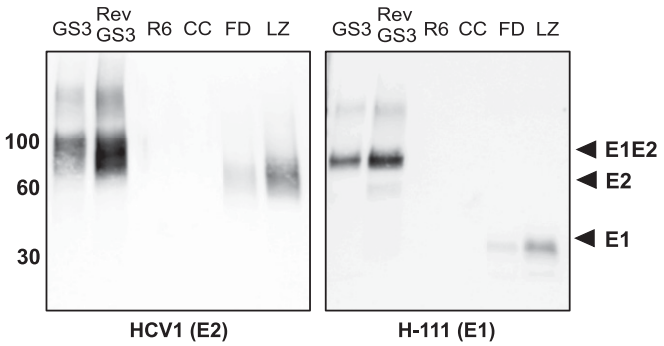

Fig. 2. E1 and E2 Western blots of sE1E2 supernatant. HCV1 antibody at 5 μg/mL was used for the E2 Western blot. H-111 antibody at 10 μg/mL was used for the E1 Western blot. All sE1E2 supernatant samples were loaded under reducing conditions. Supernatants were concentrated 10 times prior to E1 Western blot. Molecular weights, in kilodaltons, of the Western blot markers closest to observed bands are indicated on the left. Expected band positions of E1, E2, and E1E2 are indicated with black triangles on right and labeled.

confirms the heterogeneity of each protein. mbE1E2 SEC fractions probed by Western blot under nonreducing conditions showed a number of species including prominent bands corresponding to free E1 and E2 along with higher-molecular-weight aggregates. In addition, the anti-E1 nonreducing Western blot shows discrete bands corresponding to self-associating E1 dimers and trimers as observed previously (25), suggesting that, while the purified protein is a heterogenous mixture, the mixture contains a significant population of natively assembled E1E2. In contrast, under reducing conditions the E1 and E2 components migrated at the expected molecular weight for both sE1E2.LZ (*SI Appendix*, Fig. S8) and mbE1E2 (*SI Appendix*, Fig. S9) fractions, and at a molecular weight corresponding to covalently linked E1E2 in sE1E2GS3 (*SI Appendix*, Fig. S7) fractions. The spread of the bands in SDS/PAGE and Western blots is likely due to in part heterogeneity in glycoforms, as observed previously (80, 81). To examine the contribution of glycosylation to observed size distributions, we subjected the purified proteins to PNGase F cleavage to remove the glycans. An examination of the deglycosylated proteins on a nonreducing Western blot showed more species (*SI Appendix*, Fig. S10), indicating that the heterogeneity in solution we observe for all constructs is dominated by another factor, possibly disulfide cross-linking or exchange. Although these results suggest that sE1E2.LZ is closer to the expected size of a heterodimer than mbE1E2, the range of observed sizes led us to utilize more sensitive methods of characterization to examine molecular size and heterogeneity.

Analytical Characterization of Heterogeneity in Solution. sE1E2.LZ and mbE1E2 purified constructs were also characterized using analytical ultracentrifugation (AUC), which can separate a mixture of protein populations more precisely than SEC (82). A comparison of

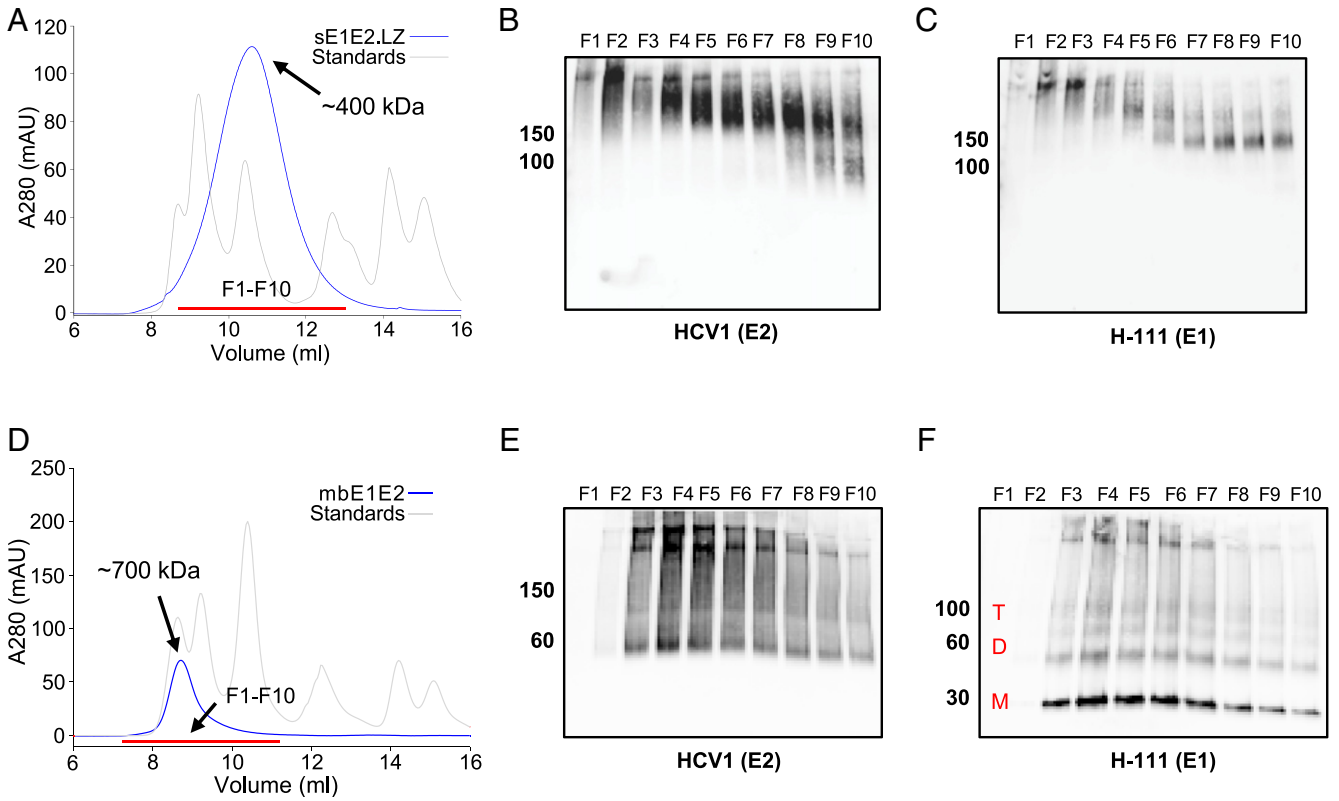

Fig. 3. SEC of sE1E2.LZ and mbE1E2. Chromatographic traces for (*A*) sE1E2.LZ and (*D*) mbE1E2 shown in blue lines plotted with molecular weight standards shown in gray lines after elution from a Superdex 200 SEC column (Cytiva). Molecular weight estimates for the center of each peak are labeled based on comparisons with elution of high-molecular-weight standards (Cytiva), with molecular masses of 670, 440, 158, 73, and 44 kDa. The range for elution fractions F1 to F10 used for analysis is shown as a red line. Western blots of sE1E2.LZ for E2 (*B*), sE1E2.LZ for E1 (*C*), mbE1E2 for E2 (*E*), and mbE1E2 for E1 (*F*) under nonreducing conditions. HCV1 antibody was used to probe for E2, while H-111 antibody was used to probe for E1. Molecular weights, in kilodaltons, of the Western blot markers closest to observed bands are indicated on the left of each panel. All fractions had 250 ng loaded for improved visualization of size. For E1 Western blots, all fractions were concentrated 10 times prior to loading. Putative E1 monomer, dimer, and trimer populations shown in *F* are highlighted with red initials.

AUC results offers further support that sE1E2.LZ is less heterogeneous than mbE1E2. AUC for sE1E2.LZ showed two prominent peaks between sedimentation coefficient (S) values 4.9 and 7.7, which are approximately consistent with a monomer and dimer of the sE1E2.LZ heterodimer, respectively, and resemble what we observe in the nonreducing Western blot. To control for potential effects of 0.5% *n*-octyl-β-D-glucopyranoside (β-OG), a detergent required for mbE1E2 purification, we performed a parallel AUC experiment with sE1E2.LZ in the presence of 0.5% β-OG (Fig. 4*A*). The size distribution in that experiment closely matched that of the sample without β-OG, indicating that the detergent itself does not contribute to heterogeneity. mbE1E2 showed three large peaks between S values 4 and 9.1, suggesting that mbE1E2 exhibits more heterogeneity than sE1E2.LZ (Fig. 4*B*). Furthermore, the peak with the highest intensity for mbE1E2 closely resembles the S value found for free E2. sE1E2.LZ, by contrast, shows no peak at that S value. Although sE1E2.LZ is not a uniform single species, it is a less complex mixture of E1E2 assemblies than mbE1E2.

SEC with multiangle light scattering (SEC-MALS) was used as another analytical technique to examine the heterogeneity and size of sE1E2.LZ. Since the presence of β-OG detergent had little to no effect on sE1E2.LZ in AUC, we expected that an absence of β-OG would not affect analytical characterization of sE1E2.LZ in SEC-MALS. When compared with standards and analyzed by light scattering, sE1E2.LZ exhibited a single peak in SEC-MALS with an estimated molecular weight at peak center of 173 kDa, corresponding approximately to a dimer of the sE1E2.LZ heterodimer (Fig. 4*C*). This estimated size is generally consistent with the observed AUC peak around 7.7 S, though the breadth of the peak in SEC-MALS still suggests that sE1E2.LZ displays some heterogeneity in size, corresponding to one to two sE1E2.LZ heterodimers, in accordance with the two major peaks from AUC measurements. In SEC-MALS, mbE1E2 was characterized as a single, very broad peak with an estimated molecular weight of 1.1 MDa at peak center (Fig. 4*D*). The broad range of this peak identified mbE1E2 as a mixture containing a broad range of species, with ~5 to over 20 E1E2 heterodimers. Additionally, sE1E2.LZ was directly compared to mbE1E2 in a native Western blot, showing differences in overall size (*SI Appendix*, Fig. S11). In assessments by multiple analytical

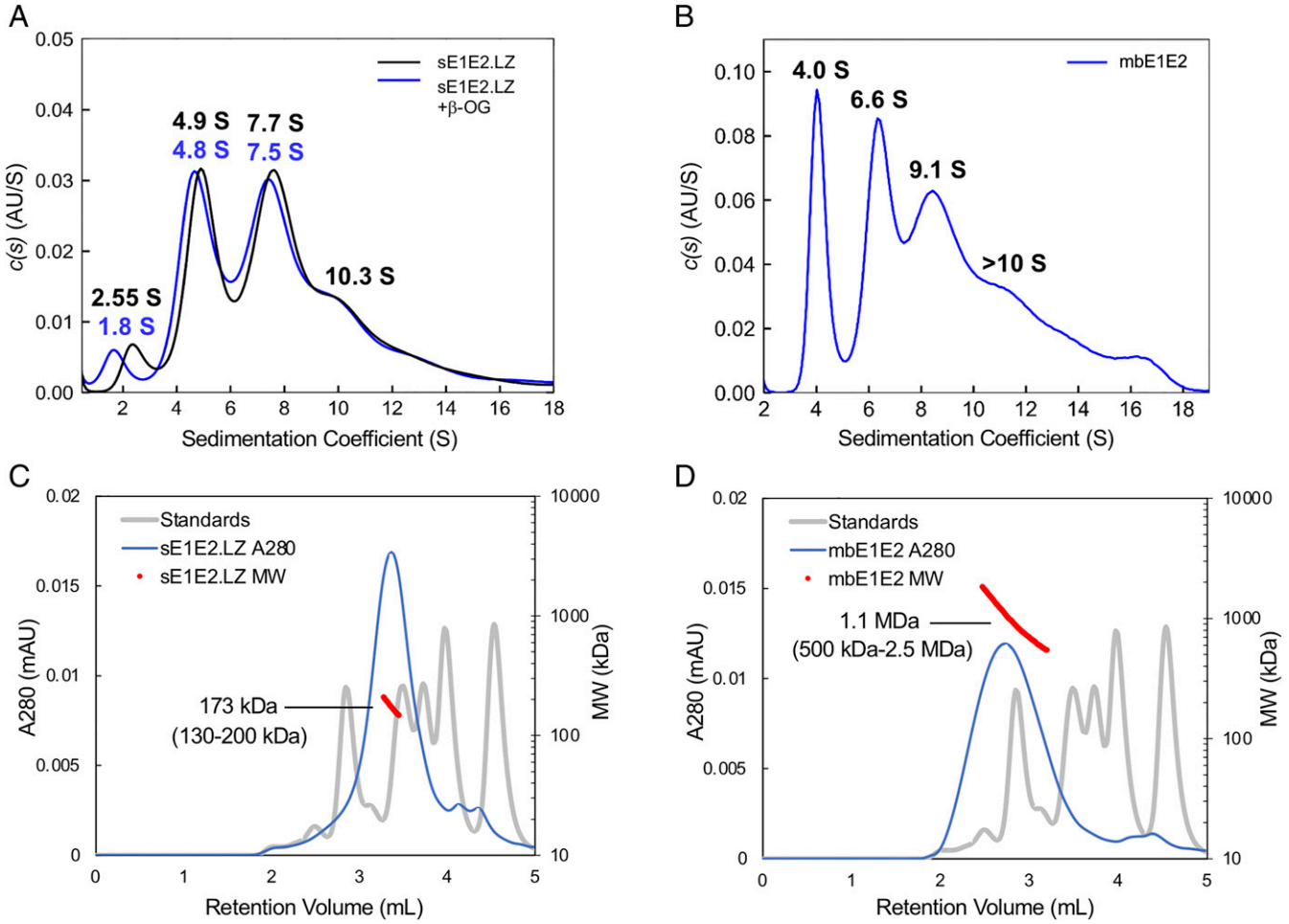

Fig. 4. Analytical characterization of sE1E2.LZ and mbE1E2 size and heterogeneity. AUC profiles of (*A*) purified sE1E2.LZ with or without detergent β-OG and (*B*) purified mbE1E2. Shown are the distribution of Lamm equation solutions *c*(*s*) for the two proteins (blue or black lines). Calculated sedimentation coefficients for the peaks are labeled. Observed species for sE1E2.LZ approximately correspond to a heterodimer at 4.9 S, a dimer of heterodimers at 7.7 S, and higher-order aggregates at 10.3 S. Observed species for mbE1E2 approximately correspond to free E2 at 4.0 S, a dimer of heterodimers at 6.6 S, a trimer of heterodimers at 9.1 S, and a tetramer of heterodimers and higher-order aggregates at >10 S. (*C*) sE1E2.LZ and (*D*) mbE1E2 characterization with SEC-MALS. The chromatographs of each protein are shown as blue lines. For reference, chromatographs of molecular weight standards are shown as gray lines in *C* and *D*, corresponding to molecular masses of 670, 158, 44, 17, and 1.35 kDa. The MALS scattering sizes between the peak half-maxima are shown as red points, with the estimated molecular weight at the center of each peak labeled and size distribution of each range in parentheses. Based on calculated molecular weights of each heterodimer and SEC-MALS molecular size ranges, these peaks predominantly contain oligomers of (*C*) 1 to 2 sE1E2.LZ heterodimers and (*D*) 5 to 27 mbE1E2 heterodimers.

techniques, sE1E2.LZ forms a moderately heterogeneous mixture that is nonetheless smaller and closer to the expected size than mbE1E2, representing a potentially improved immunogen for HCV vaccine development and a candidate for structural characterization. In addition, sE1E2.LZ does not require detergents for solubility, allowing for simpler formulations than mbE1E2.

sE1E2.LZ Exhibits Native-Like E1E2 Antigenicity and Robust Immunogenicity. We next examined the native-like properties of sE1E2.LZ by measuring the binding affinities to a panel of bnAbs in comparison with secreted E2 ectodomain (sE2) and mbE1E2. Unlike the antibodies used in Western blot, most bnAbs used for this analysis recognize conformational epitopes on E2 (41, 83, 84) and E1E2 (46). We first performed an enzyme-linked immunosorbent assay (ELISA) at one antibody concentration to compare mbE1E2 and sE1E2.LZ antibody reactivity, along with purified sE1E2GS3 and sE2. This screening was used to assess lack of reactivity by any of the constructs to conformationally sensitive antibodies, versus quantitative comparisons of affinities, which was undertaken later. The antibodies utilized were a representative panel of bnAbs to antigenic domain B, D, and E epitopes in E2 and the E1E2 bnAbs AR4A and AR5A (Fig. 5). At the tested antibody concentration (0.185 μg/mL), mbE1E2 and sE1E2.LZ exhibited similar binding levels for all antibodies. Importantly, sE1E2.LZ maintained reactivity to E1E2 bnAbs, providing evidence that this sE1E2 construct contains a soluble, native-like form of the E1E2 heterodimer. In contrast, sE1E2GS3 and sE2 showed little to no reactivity to AR4A and AR5A; this was not unexpected for sE2, which lacks key residues comprising the E1E2 bnAb epitopes (85). Based on the AR4A and AR5A binding results, the lack of E1–E2 cleavage or scaffold in sE1E2GS3 appears to lead to a severe disruption of native-like assembly, and thus we focused on sE1E2.LZ for subsequent characterization.

To confirm more precisely our initial measurements of bnAb reactivity, we tested the affinity of sE1E2.LZ to a larger panel of HCV antibodies (Table 1) and CD81 (Fig. 6). Dissociation constants (K_ds) were measured by dose-dependent ELISA to antibodies that recognize discrete epitopes of E2 (18) and E1E2 bnAbs. For comparison, we performed the same analysis for purified mbE1E2 and sE2. sE1E2.LZ and mbE1E2 showed similar affinities to almost all tested HCV HMAbs, within a two- to threefold difference. One notable exception was an eightfold lower affinity of AR4A for sE1E2.LZ relative to mbE1E2. Although sE1E2.LZ maintained affinity to AR5A, a decrease in affinity to AR4A may stem from subtle differences in heterodimer assembly or dynamics when compared to mbE1E2, which may be difficult to elucidate without detailed structural characterization of the epitope. Regardless, AR4A binds sE1E2.LZ with nanomolar affinity (16 nM), indicating that the overall structure of the AR4A epitope and the E1E2 interface in that region are intact. In addition to measurements of binding to conformationally sensitive E2 and E1E2 HMAbs, we also tested binding to the CD81 receptor, which recognizes a region on the E2 ectodomain overlapping with epitopes for a number of bnAbs (85). sE1E2.LZ showed robust binding to the large extracellular loop (LEL) of CD81 in surface plasmon resonance (SPR) (10.8 nM; Fig. 6), establishing that this sE1E2 construct displays receptor binding critical for native HCV infection. While measured CD81-LEL K_d values show comparable and in some cases higher affinity than corresponding glycoprotein affinities for antibodies in Table 1, due to the different experimental measurement methods, these results provide a comparison between antigens rather than a comparison between absolute glycoprotein affinities of receptor versus antibodies.

Table 1. Binding affinity of mbE1E2, sE1E2.LZ, and sE2 to panel of monoclonal antibodies measured by dose-dependent ELISA, with standard error (SE) values shown for each affinity measurement

		K_d, nM			SE, nM		
Antibody	Domain*	mbE1E2	sE1E2.LZ	sE2	mbE1E2	sE1E2.LZ	sE2
CBH-4D	A	28	26	1	3.2	3.4	0.2
CBH-4G	A	7.8	18	0.5	2.3	3.1	0.3
HC-1 AM†	B	1.5	2.9	3.6	0.06	0.5	0.4
HC-11	B	1.8	3.2	11	0.09	0.4	0.6
CBH-7	C	1	1.7	0.3	0.1	0.1	0.04
HC84.24	D	0.5	1.3	0.7	0.07	0.1	0.1
HC84.26	D	1.2	2.6	0.4	0.03	0.4	0.1
HC33.1	E	3.8	0.9	1.9	0.3	0.09	0.2
HCV1	E	9.8	3.5	6.2	0.3	0.2	0.3
AR4A	E1E2	2.3	16	—	0.2	1.5	—
AR5A	E1E2	1.5	1.7	—	0.2	0.2	—

Dashes denote no binding detected.
*Antigenic domain on E2 targeted by antibody (A–E), as previously described (86). "E1E2" denotes antibodies that target the E1E2 heterodimer.
†Affinity-matured HC-1 antibody, as previously described (87).

After confirming the native-like antigenicity of sE1E2.LZ, we tested the native-like properties of sE1E2.LZ in vivo to determine whether it will elicit antibodies that effectively recognize HCV and inhibit infection. Mice were immunized with either mbE1E2, sE1E2.LZ, or sE2 and tested for the presence of antibodies that target E1E2 and neutralize the virus (Fig. 7). sE1E2.LZ elicited anti-mbE1E2 antibody responses that were similar to responses from mbE1E2-immunized mice, while serum binding of mbE1E2 from sE2-immunized mice was lower, in particular compared with the mbE1E2-immunized group ($P \leq 0.01$) (Fig. 7*A*). Binding of immunized sera to H77C-pseudotyped HCV pseudoparticles (HCVpp) was also tested for all groups (Fig. 7*B*), and while mean serum titer was highest for the sE1E2.LZ group, there were no significant differences found between immunized group titers based on nonparametric (Kruskal–Wallis) assessment. Serum neutralization of H77C HCVpp was tested for all groups to assess for elicitation of neutralizing antibodies that target the

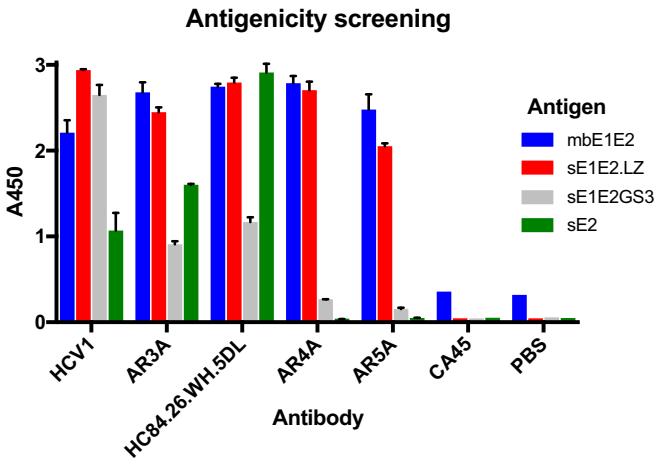

Fig. 5. Initial antigenicity screening of sE1E2 designs in ELISA. mbE1E2, sE1E2.LZ, sE1E2GS3, and sE2 were coated on ELISA plates at a concentration of 2 μg/mL and tested for binding to a panel of E2 and E1E2 bnAbs, representing E2 antigenic domains E (HCV1), B (AR3A), and D (HC84.26.WH.5DL), as well as E1E2 domains AR4 (AR4A) and AR5 (AR5A). Binding was measured at 450 nm with an antibody concentration of 0.185 μg/mL. Negative controls shown are an unrelated antibody (CA45) or PBS.

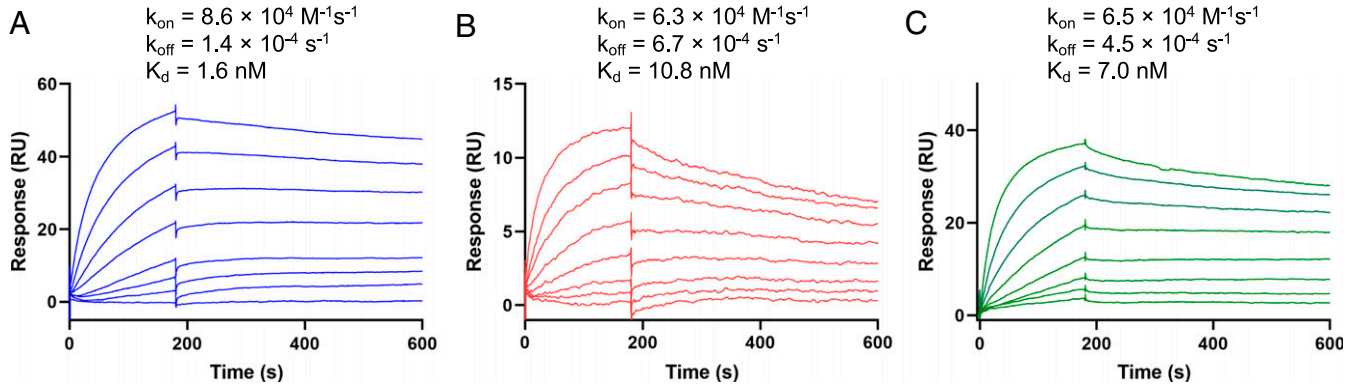

Fig. 6. Measurement of binding to the CD81 receptor by SPR. CD81 binding kinetic curves to (*A*) mbE1E2, (*B*) sE1E2.LZ, and (*C*) sE2 are shown. Kinetic (k_{on}, k_{off}) and steady-state (K_d; calculated as k_{off}/k_{on}) binding parameters were calculated based on 1:1 model and are shown in each panel.

homologous virus (Fig. 7*C*). Testing of preimmune sera for background neutralization showed no detectable HCVpp neutralization (*SI Appendix*, Fig. S12). sE1E2.LZ-immunized sera showed robust neutralization of HCVpp, with neutralization titers (half-maximal inhibitory dose, ID_{50}) that showed no significant difference from mbE1E2-immunized and sE2-immunized groups. This initial test of sE1E2.LZ immunogenicity shows that this secreted E1E2 construct is able to induce an antibody response comparable to mbE1E2 and sE2 that can recognize homologous E1E2 on the surface of HCVpp and neutralize the virus.

Discussion

The development and characterization of a native-like E1E2 antigen containing a leucine zipper scaffold offers a proof-of-principle platform for designing E1E2 vaccine antigens within a soluble and secreted backbone. Exploration of this scaffold approach for the production of E1E2 from other HCV genotypes is warranted, as sE1E2.LZ was only designed using the H77C sequence. E2 ectodomains from other strains have been characterized structurally (39, 54, 88), and the E1E2 sequences of those strains could be targets for sE1E2.LZ backbone expression and characterization. However, strain-specific sequence changes may affect sE1E2.LZ secretion, as differences in E1 and E2 stalk regions could modulate assembly and export from cellular components (89, 90). In addition, further studies of sE1E2 secretion may shed light on cellular factors that facilitate efficient sE1E2 assembly, which could then be used either to improve production levels or to examine mechanisms of viral assembly and secretion.

There are several avenues for subsequent design and optimization of the sE1E2.LZ platform. As a potential vaccine immunogen, the human leucine zipper of sE1E2.LZ poses potential problems related to immunizing humans with human protein sequences (91, 92). As the c-Jun/c-Fos leucine zipper is structurally defined at high resolution, this can be used as a template for identification of heterodimeric leucine zipper structures from nonhuman proteins or de novo designs of synthetic leucine zipper scaffolds. Furthermore, although the CC1+CC2 sE1E2 design (sE1E2.CC) did not yield appreciable secretion, it is possible that alternative heterohexameric scaffolds, possibly generated using c-Jun/c-Fos leucine zipper structure as a subunit, could promote stable E1E2 assembly. Finally, recent studies have shown that cage-like protein nanoparticles can provide scaffolds for viral glycoproteins such as RSV F (93, 94) and influenza hemagglutinin (57). A nanoparticle recapitulating the c-Jun/c-Fos leucine zipper structure as attachment points could be identified or designed to present sE1E2 in a similar nanoparticle format. Binding to E1E2-specific antibodies, such as AR4A and AR5A, is particularly important for validation of scaffolded E1E2 antigens. Since sE1E2.LZ exhibited slightly impaired binding to AR4A, new designed or synthetic scaffolds may provide an opportunity to improve upon the human leucine zipper scaffold by matching or exceeding wild-type binding to

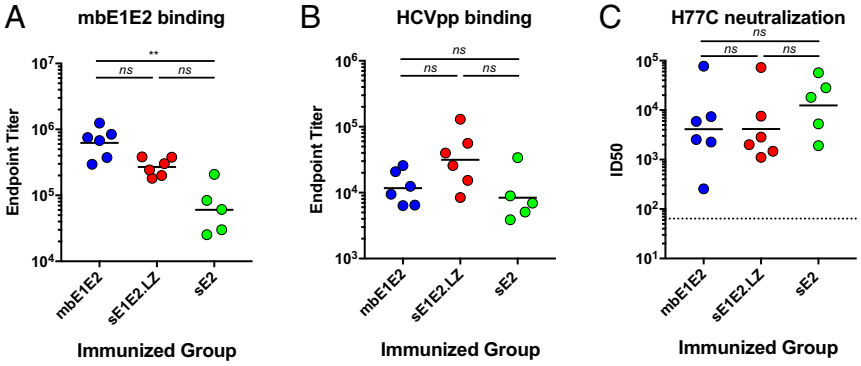

Fig. 7. Immunogenicity assessment of sE2, mbE1E2, and sE1E2.LZ. Six mice per group were immunized with sE2, mbE1E2, or sE1E2.LZ, and sera were tested for binding to (*A*) mbE1E2 and (*B*) H77C-pseudotyped HCVpp in ELISA. One mouse in the sE2-immunized group died prior to final bleed, and thus responses for five mice are shown for that group. Endpoint titers were calculated using Graphpad Prism, and geometric mean titers are shown for each group as black lines. (*C*) Neutralization of H77C HCVpp by immunized murine sera. ID_{50} values were calculated in Graphpad Prism for individual mice, and average ID_{50} titers for each immunized group are shown as black lines. The minimal serum dilution used for ID_{50} measurement (1:64) is shown as a horizontal dashed line, for reference. *P* values between group endpoint titer or ID_{50} values were calculated using Kruskal–Wallis analysis of variance with Dunn's multiple comparison test (*ns*, not significant: $P > 0.05$; $^{**}P \leq 0.01$).

E1E2-specific antibodies. High-resolution structural characterization of sE1E2.LZ or subsequent designs, enabled by effective secretion and purification of this native-like assembly, can permit an improved view of the determinants of E1E2 assembly and support structure-based modifications to enhance assembly and stability.

Although sE1E2.LZ was observed as closer to expected size of a heterodimer than mbE1E2, our extensive analytical characterization indicated a likely mix of heterodimers and higher-order oligomers. This degree of sample heterogeneity has been found during purification of previous soluble construct designs, both with a covalent linker (68) and a designed heterodimeric scaffold (71). Although glycoform heterogeneity is apparent in both constructs, our results suggest that it is not the primary source of observed oligomerization. Instead, these constructs demonstrate that removing the heterodimer from its natural membrane-attached environment does not preclude formation of large assemblies. The E2 ectodomain likely plays a large role in aggregation via additional hydrophobic interactions or disulfide cross-linking, as its ectodomain contains conserved and surface-exposed tyrosines, tryptophans, and cysteines (18). These residues are critical for coreceptor interactions (36, 95), proper ectodomain folding, and assembly (85, 89) but could readily mediate E1E2 aggregation without TMDs present. Self-association of E2 ectodomains has also been noted previously (96), offering additional support for the propensity of soluble E2 to exhibit cross-linking. Future studies will examine specific determinants of sE1E2.LZ heterogeneity and methods to mitigate it, building on recent efforts to obtain homogenous secreted glycoprotein (97). Experimental structural characterization, as noted above, would help to delineate the stoichiometry and oligomerization modes of sE1E2 designs.

In summary, replacing the native TMDs of E1 and E2 with a leucine zipper scaffold provides proof of concept that this approach can be used to develop a native-like, antigenically and immunogenically intact E1E2 complex without requiring a membrane or detergent environment. The design and validation of additional scaffolds that adopt dimeric, trimeric, or heterohexameric quaternary structures could elucidate key determinants of E1E2 complex assembly, another area of research that has been hindered by membrane association of E1E2. In addition, this scaffold approach could serve as a platform to study how the substantial genetic diversity of HCV translates to structural diversity and envelope glycoprotein dynamics, and how structural and dynamic changes, including "open" and "closed" envelope glycoprotein states, may promote immune evasion, as noted by recent work (98). Finally, in addition to their use in structural characterization, designed soluble E1E2 complexes with functional TMD replacements that retain all essential structural properties can serve as an integral component of rational vaccine design.

Materials and Methods

Protein Expression. For expression of recombinant soluble HCV E2 (sE2), the sequence from isolate H77C (GenBank accession number AF011751; residues 384 to 661) was cloned into the pSecTag2 vector (Invitrogen)* and expressed in mammalian (Expi293F) cells as described previously (99). The mbE1E2 and sE1E2 DNA coding sequences were synthesized with a modified tPA signal peptide (72) at the N terminus. All E1E2 sequences were cloned into the vector pcDNA3.1+ at the cloning sites of KpnI/NotI (GenScript). Furin sequence DNA was cloned into the vector pcDNA3.1 and was a gift from Yuxing Li, University of Maryland Institute for Bioscience and Biotechnology Research, Rockville, MD. All sE1E2 constructs and mbE1E2 were transfected with ExpiFectamine 293 into Expi293F cells for expression (Invitrogen). Cleavable polyprotein constructs were cotransfected with the furin construct at a 2:1 ratio. A clone for mammalian expression of CD81-LEL, containing N-terminal tPA signal sequence and C-terminal twin Strep tag, was provided by Joe Grove, University College London, London. CD81-LEL was expressed through transient transfection in Expi293F cells (Thermo Fisher Scientific).

Antibodies. mAbs used in ELISA and binding studies were produced as previously described (83, 100, 101), with the exception of AR4A and AR5A, which were kindly provided by Mansun Law, Scripps Research Institute, La Jolla, CA.

Protein Purification and SEC. sE2 glycoprotein was purified from cell supernatant as described previously (99). Culture supernatant of sE1E2.LZ and sE1E2GS3 was purified by IMAC with separate HiTrap chelating HP Ni^{2+}-NTA columns (Cytiva). Expressed mbE1E2 was extracted from cell membranes using 1% NP-9 and purified via sequential Fractogel EMD TMAE (Millipore), Fractogel EMD SO_3^- (Millipore), HC84.26 immunoaffinity (102), and agarose-linked *Galanthus nivalis* lectin (GNA; Vector Laboratories) affinity chromatography. Sample concentration prior to SEC was conducted with 15 mL Amicon Ultra 3-kDa centrifugal filters (Millipore Sigma). sE1E2.LZ, sE1E2GS3, and mbE1E2 were fractionated using a Superdex 200 Increase 10/300 column (Cytiva). sE1E2.LZ and sE1E2GS3 were equilibrated with 1× phosphate-buffered saline (PBS; 10 mM sodium phosphate + 150 mM NaCl), pH 7, and mbE1E2 was equilibrated in Tris-buffered saline (TBS; 25 mM Tris·HCl + 150 mM NaCl), pH 7.5 + 0.5% β-OG (Anatrace). Size-exclusion fractions of 500 μL were collected on AKTA FPLC (Cytiva). Molecular weight standards from the high-molecular-weight calibration kit (Cytiva) were compared to purified sE1E2.LZ, sE1E2GS3, and mbE1E2.

SEC-MALS. For SEC-MALS, a UHPLC system (Vanquish Flex; Thermo Fisher) was coupled to MALS (DAWN HELEOS-II, Wyatt) and Refractive Index (Optilab T-rEX; Wyatt) detectors. Separations were performed using a WTC-050N5 column (Wyatt) equilibrated in PBS for sE1E2.LZ or in TBS + 0.5% β-OG for mbE1E2, with a flow rate of 0.3 mL/min and sample injection volumes of 25 μL. Molar mass analysis was performed using the software ASTRA 7.1.3 (Wyatt) using refractive index as a concentration source.

SDS/PAGE and Western Blot. SDS/PAGE and Western blot experiments were conducted with 12-well stain-free gels (Bio-Rad), with total protein detected using a stain-free imager (Bio-Rad). For SDS/PAGE, Precision Plus Unstained Protein Standards (Bio-Rad) were used as a molecular weight marker. E2 was detected in Western Blot with HCV1 (79) as the primary antibody. E1 was detected in Western blot with H-111 as the primary antibody (78). In reducing conditions, each sample was incubated with loading dye (4× Laemmli buffer + 10% β-mercaptoethanol) (Bio-Rad) and heated to 95 °C, with the exception of mbE1E2, which was heated to 37 °C. In nonreducing conditions, each sample was incubated with Laemmli buffer and heated to 37 °C. For Western blots, stain-free gels were transferred to a turbo mini 0.2 μm nitrocellulose membrane (Bio-Rad) using the transblot turbo transfer system (Bio-Rad). Supersignal Molecular Weight Protein Ladder (Thermo Fisher Scientific) was used as a marker for Western blots. The 10× concentration of supernatant for E1 Western blots was conducted in 0.5 mL Amicon Ultra 3-kDa centrifugal filters (Millipore Sigma). Cell lysates of sE1E2.LZ and mbE1E2 were collected by centrifugation of 1 mL transfected cell suspension and extraction from cell membranes with 1% NP-9. For native Western blots, 15-well NativePAGE Novex 4 to 16% Bis-Tris protein gels (Thermo Fisher Scientific) were transferred to a turbo mini 0.2-μm polyvinylidene difluoride membrane (Bio-Rad) using the same transfer system. NativeMark unstained protein standard (Invitrogen) was used as a molecular weight marker for native gels. To deglycosylate sE1E2.LZ, mbE1E2, and sE2 in nonreducing conditions, 3 μg of each protein was mixed with 2 μL PNGase F enzyme (New England Biolabs) then incubated at 37 °C for 24 h before Western blot preparation. Proteins were detected with goat anti-human IgG horseradish peroxidase (HRP) conjugate (Invitrogen) and Clarity Western ECL Substrate (Bio-Rad). All gels were imaged using the ChemiDoc system (Bio-Rad).

AUC. Sedimentation velocity (SV) experiments were performed at 20 °C using a ProteomeLab Beckman XL-A with absorbance optical system and a four-hole An60-Ti rotor (Beckman Coulter). For sE1E2.LZ, the sample and reference sectors of the dual-sector charcoal-filled epon centerpieces were loaded with 390 μL protein in PBS, pH 7.4, with or without 0.5% β-OG, and 400 μL buffer. For mbE1E2, the sample and reference sectors of the dual-sector charcoal-filled epon centerpieces were loaded with 390 μL protein in

*Certain commercial equipment, instruments, or materials are identified in this paper in order to specify the experimental procedure adequately. Such identification is not intended to imply recommendation or endorsement by the National Institute of Standards and Technology, nor is it intended to imply that the materials or equipment identified are necessarily the best available for the purpose.

TBS + 0.5% β-OG and 400 μL buffer. The cells were centrifuged at 40,000 rpm and the absorbance data were collected at 280 nm in a continuous mode with a step size of 0.003 cm and a single reading per step to obtain linear signals of <1.25 absorbance units. Sedimentation coefficients were calculated from SV profiles using the program SEDFIT (103). The continuous *c*(*s*) distributions were calculated assuming a direct sedimentation boundary model with maximum entry regularization at a confidence level of 1 SD. The density and viscosity of buffers at 20 °C and 4 °C were calculated using SEDNTERP (104). The *c*(*s*) distribution profiles were prepared with the program GUSSI (C. A. Brautigam, University of Texas Southwestern Medical Center).

ELISA. HCV HMAb binding to mbE1E2, sE1E2.LZ, sE1E2GS3, and sE2 were evaluated and quantitated by ELISA. Ninety-six-well microplates (MaxiSorp; Thermo Fisher) were coated with 5 μg/mL *Galanthus nivalis* lectin (GNL; Vector Laboratories) overnight, and purified mbE1E2, sE1E2.LZ, sE1E2GS3 and sE2 was then added to the plates at 2 μg/mL. After the plates were washed with PBS and 0.05% Tween 20 and blocked by Pierce Protein-Free (PBS) Blocking Buffer (Thermo Fisher), the mAbs were tested in duplicate at threefold serial dilution starting at 100 μg/mL. The binding was detected by 1:5,000 dilutions of HRP-conjugated anti-human IgG secondary antibody (Invitrogen) with TMB substrate (Bio-Rad). The absorbance was read at 450 nm using a SpectraMax MS microplate reader (Molecular Devices). For ELISA measurements of immunized murine sera, endpoint titers were calculated by curve fitting in GraphPad Prism software, with endpoint optical density defined as four times the mean absorbance value of day 0 sera.

Determination of Antibody Affinity by Quantitative ELISA. ELISA was performed as described (83) to compare antibody affinity to sE1E2.LZ, mbE1E2, and sE2. Briefly, plates were developed by coating wells with 500 ng of GNL and blocking with 2.5% nonfat dry milk and 2.5% normal goat serum. Purified sE1E2.LZ, mbE1E2, and sE2 at 5 μg/mL were captured by GNA onto the plate and later bound by a range of 0.01 to 200 μg/mL of antibody. Bound antibodies were detected by incubation with alkaline phosphatase-conjugated goat anti-human IgG (Promega), followed by incubation with *p*-nitrophenyl phosphate for color development. Absorbance was measured at 405 nm and 570 nm. The assay was carried out in triplicate in three independent assays for each HMAb. The data were analyzed by nonlinear regression to measure antibody K_ds and binding potential (optical density at 405 nm) using Graphpad Prism software, and standard error (SE) values were calculated using the three independent affinity measurements.

SPR. SPR analysis was performed using a Biacore T200 system (Cytiva) and HBS-EP+ buffer was used as sample and running buffer. The analysis temperature and sample compartment were set to 25 °C. mbE1E2, sE2, and sE1E2.LZ were immobilized on Series S CM5 chips using the Amine Coupling Kit per the manufacturer's instructions. Antigen capture levels were adjusted to yield ∼2,000 response units (RU) for the kinetic experiments. Purified CD81-LEL was injected over reference and active flow cells, applying a single cycle kinetics procedure using twelve concentrations. Data were fitted to a 1:1 binding model using Biacore T200 Evaluation Software 2.0. As one concentration series was used to calculate binding parameters no SEs were calculated for those values.

Animal Immunization. CD-1 mice were purchased from Charles River Laboratories. Prior to immunization, sE2 and E1E2 antigens were formulated with polyphosphazene PCPP-R adjuvant (105). Poly[di(carboxylatophenoxy)phosphazene], PCPP (50 μg, molecular weight 800,000 Da) (106) was formulated with resiquimod, R848 (25 μg) in PBS (pH 7.4) to prepare PCPP-R as described previously (105). The resulting formulation was mixed with E1E2 (70 μg for prime or 15 μg for boost immunization) or sE2 antigen (50 μg for prime or 10 μg for boost immunization), with antigen amounts selected to ensure approximate molar equivalence of E2 in the vaccines. The absence of aggregation in adjuvanted formulations was confirmed by dynamic light scattering. The formation of antigen–PCPP-R complex was confirmed by asymmetric flow field flow fractionation (AF4) as described previously (107). Groups of six female mice, age 7 to 9 weeks at study start, were injected via the intraperitoneal (IP) route for prime (day 0) and boost (days 14, 28, and 42) immunizations. Blood samples were collected prior to each injection with a terminal bleed on day 56. The collected samples were processed for serum by centrifugation and stored at −80 °C until analysis was performed. The in vivo work was conducted in the AAALAC and USDA Animal Welfare Act compliant vivarium of Noble Life Sciences, Inc. (NLS, Sykesville, Maryland) and monitored by NLS IACUC (NIH OLAW Assurance # D16-00845 [A4633-01]).

HCVpp Generation. HCVpp were generated as described previously (81), by cotransfection of HEK293T cells with the murine leukemia virus Gag-Pol packaging vector, luciferase reporter plasmid, and plasmid expressing HCV E1E2 using Lipofectamine 3000 (Thermo Fisher Scientific). Envelope-free control (empty plasmid) was used as a negative control in all experiments. Supernatants containing HCVpp were harvested at 48 h and 72 h post-transfection and filtered through 0.45-μm-pore membranes. For measurements of serum binding to HCVpp in ELISA, concentrated HCVpp were obtained by ultracentrifugation of 33 mL of filtered supernatants through a 7-mL 20% sucrose cushion using an SW 28 Beckman Coulter rotor at 25,000 rpm for 2.5 h at 4 °C, following a previously reported protocol (42).

HCVpp Neutralization Assays. Huh7 cells were maintained in the Dulbecco's modified Eagle's medium (DMEM) supplemented with 10% fetal bovine serum; 1.5×10^4 Huh7 cells per well were plated in white 96-well tissue culture plates (Corning) and incubated overnight at 37 °C. The following day, HCVpp was mixed with serial diluted murine serum samples at 37 °C. After 1-h incubation, the HCVpp–serum mixture was added to the Huh7 cells (kindly provided by Jonathan K. Ball, University of Nottingham, Nottingham, UK) in 96-well plates and incubated at 37 °C for 5 h. After removing the inoculum, the cells were further incubated for 72 h with DMEM containing 10% fetal bovine serum (Thermo Fisher) and the luciferase activities were measured using Bright-Glo luciferase assay system as indicated by the manufacturer (Promega).

Statistical Comparisons. *P* values between group endpoint titers and group ID_{50} values were calculated in Graphpad Prism software, using nonparametric Kruskal–Wallis analysis of variance with Dunn's multiple comparisons test.

Data Availability. All study data are included in the paper and *SI Appendix*.

ACKNOWLEDGMENTS. We thank Dr. Yuxing Li and Chi-I Chiang (University of Maryland Institute for Bioscience and Biotechnology Research [IBBR]) for providing the furin protein expression construct and for useful discussions regarding its use for glycoprotein expression. We are also grateful to Dr. Joe Grove (University College London) for providing the CD81-LEL expression construct, Melissa Kerzic (University of Maryland IBBR) for helpful suggestions regarding sE1E2 construct design, and Peilong Lu (University of Washington Institute for Protein Design) for suggestions regarding coiled-coil peptide design and assessment. Gilad Ofek (University of Maryland IBBR) provided assistance with the SPR experiments and Liudmila Kulakova (University of Maryland IBBR) provided assistance with Western blots. This work was supported by NIH R01 AI132213 (to B.G.P., A.K.A., R.A.M., S.K.H.F., and T.R.F.), R21 AI154100 (to B.G.P., E.A.T., and T.R.F.), U19-AI123862 (to S.K.H.F.), and MPower Maryland (to A.K.A., R.A.M., B.G.P., and T.R.F.).

1. WHO, "Global hepatitis report 2017" (World Health Organization, Geneva, 2017).
2. Y. Waheed, M. Siddiq, Z. Jamil, M. H. Najmi, Hepatitis elimination by 2030: Progress and challenges. *World J. Gastroenterol.* **24**, 4959–4961 (2018).
3. S. H. Moosavy *et al*., Epidemiology, transmission, diagnosis, and outcome of hepatitis C virus infection. *Electron. Physician* **9**, 5646–5656 (2017).
4. S. Zaltron, A. Spinetti, L. Biasi, C. Baiguera, F. Castelli, Chronic HCV infection: Epidemiological and clinical relevance. *BMC Infect. Dis.* **12** (suppl. 2), S2 (2012).
5. F. Ansaldi, A. Orsi, L. Sticchi, B. Bruzzone, G. Icardi, Hepatitis C virus in the new era: Perspectives in epidemiology, prevention, diagnostics and predictors of response to therapy. *World J. Gastroenterol.* **20**, 9633–9652 (2014).
6. S. Bühler, R. Bartenschlager, Promotion of hepatocellular carcinoma by hepatitis C virus. *Dig. Dis.* **30**, 445–452 (2012).
7. R. Bartenschlager *et al*., Critical challenges and emerging opportunities in hepatitis C virus research in an era of potent antiviral therapy: Considerations for scientists and funding agencies. *Virus Res.* **248**, 53–62 (2018).
8. A. Al-Khazraji *et al*., Identifying barriers to the treatment of chronic hepatitis C infection. *Dig. Dis.* **38**, 46–52 (2020).
9. B. Roche, A. Coilly, J. C. Duclos-Vallee, D. Samuel, The impact of treatment of hepatitis C with DAAs on the occurrence of HCC. *Liver Int.* **38** (suppl. 1), 139–145 (2018).
10. H. Midgard *et al*., Hepatitis C reinfection after sustained virological response. *J. Hepatol.* **64**, 1020–1026 (2016).
11. J. D. Duncan, R. A. Urbanowicz, A. W. Tarr, J. K. Ball, Hepatitis C virus vaccine: Challenges and prospects. *Vaccines (Basel)* **8**, E90 (2020).
12. J. R. Bailey, E. Barnes, A. L. Cox, Approaches, progress, and challenges to hepatitis C vaccine development. *Gastroenterology* **156**, 418–430 (2019).

13. D. B. Smith *et al*., Expanded classification of hepatitis C virus into 7 genotypes and 67 subtypes: Updated criteria and genotype assignment web resource. *Hepatology* **59**, 318–327 (2014).
14. M. Lavie, X. Hanoulle, J. Dubuisson, Glycan shielding and modulation of hepatitis C virus neutralizing antibodies. *Front. Immunol.* **9**, 910 (2018).
15. F. Helle *et al*., Role of N-linked glycans in the functions of hepatitis C virus envelope proteins incorporated into infectious virions. *J. Virol.* **84**, 11905–11915 (2010).
16. N. A. Brasher *et al*., B cell immunodominance in primary hepatitis C virus infection. *J. Hepatol.* **72**, 670–679 (2020).
17. S. B. Cashman, B. D. Marsden, L. B. Dustin, The humoral immune response to HCV: Understanding is key to vaccine development. *Front. Immunol.* **5**, 550 (2014).
18. B. G. Pierce, Z. Y. Keck, S. K. Foung, Viral evasion and challenges of hepatitis C virus vaccine development. *Curr. Opin. Virol.* **20**, 55–63 (2016).
19. J. Prentoe, J. Bukh, Hypervariable region 1 in envelope protein 2 of hepatitis C virus: A linchpin in neutralizing antibody evasion and viral entry. *Front. Immunol.* **9**, 2146 (2018).
20. D. Sepulveda-Crespo, S. Resino, I. Martinez, Hepatitis C virus vaccine design: Focus on the humoral immune response. *J. Biomed. Sci.* **27**, 78 (2020).
21. L. Kong, K. N. Jackson, I. A. Wilson, M. Law, Capitalizing on knowledge of hepatitis C virus neutralizing epitopes for rational vaccine design. *Curr. Opin. Virol.* **11**, 148–157 (2015).
22. F. Penin, J. Dubuisson, F. A. Rey, D. Moradpour, J. M. Pawlotsky, Structural biology of hepatitis C virus. *Hepatology* **39**, 5–19 (2004).
23. D. Lapa, A. R. Garbuglia, M. R. Capobianchi, P. Del Porto, Hepatitis C virus genetic variability, human immune response, and genome polymorphisms: Which is the interplay? *Cells* **8**, E305 (2019).
24. M. Lavie, A. Goffard, J. Dubuisson, Assembly of a functional HCV glycoprotein heterodimer. *Curr. Issues Mol. Biol.* **9**, 71–86 (2007).
25. P. Falson *et al*., Hepatitis C virus envelope glycoprotein E1 forms trimers at the surface of the virion. *J. Virol.* **89**, 10333–10346 (2015).
26. L. Cocquerel, C. Wychowski, F. Minner, F. Penin, J. Dubuisson, Charged residues in the transmembrane domains of hepatitis C virus glycoproteins play a major role in the processing, subcellular localization, and assembly of these envelope proteins. *J. Virol.* **74**, 3623–3633 (2000).
27. A. Op De Beeck *et al*., The transmembrane domains of hepatitis C virus envelope glycoproteins E1 and E2 play a major role in heterodimerization. *J. Biol. Chem.* **275**, 31428–31437 (2000).
28. A. Bianchi, S. Crotta, M. Brazzoli, S. K. Foung, M. Merola, Hepatitis C virus e2 protein ectodomain is essential for assembly of infectious virions. *Int. J. Hepatol.* **2011**, 968161 (2011).
29. J. G. Haddad *et al*., Identification of novel functions for hepatitis C virus envelope glycoprotein E1 in virus entry and assembly. *J. Virol.* **91**, e00048-17 (2017).
30. G. Vieyres, J. Dubuisson, T. Pietschmann, Incorporation of hepatitis C virus E1 and E2 glycoproteins: The keystones on a peculiar virion. *Viruses* **6**, 1149–1187 (2014).
31. C. C. Colpitts, P. L. Tsai, M. B. Zeisel, Hepatitis C virus entry: An intriguingly complex and highly regulated process. *Int. J. Mol. Sci.* **21**, E2091 (2020).
32. M. B. Zeisel, D. J. Felmlee, T. F. Baumert, Hepatitis C virus entry. *Curr. Top. Microbiol. Immunol.* **369**, 87–112 (2013).
33. P. Pileri *et al*., Binding of hepatitis C virus to CD81. *Science* **282**, 938–941 (1998).
34. E. Scarselli *et al*., The human scavenger receptor class B type I is a novel candidate receptor for the hepatitis C virus. *EMBO J.* **21**, 5017–5025 (2002).
35. V. J. Kinchen *et al*., Plasma deconvolution identifies broadly neutralizing antibodies associated with hepatitis C virus clearance. *J. Clin. Invest.* **129**, 4786–4796 (2019).
36. N. Tzarum, I. A. Wilson, M. Law, The neutralizing face of hepatitis C virus E2 envelope glycoprotein. *Front. Immunol.* **9**, 1315 (2018).
37. Y. Wang, Z. Y. Keck, S. K. Foung, Neutralizing antibody response to hepatitis C virus. *Viruses* **3**, 2127–2145 (2011).
38. M. D. Colbert *et al*., Broadly neutralizing antibodies targeting new sites of vulnerability in hepatitis C virus E1E2. *J. Virol.* **93**, e02070-18 (2019).
39. A. I. Flyak *et al*., HCV broadly neutralizing antibodies use a CDRH3 disulfide motif to recognize an E2 glycoprotein site that can Be targeted for vaccine design. *Cell Host Microbe* **24**, 703–716.e3 (2018).
40. Z. Y. Keck *et al*., Broadly neutralizing antibodies from an individual that naturally cleared multiple hepatitis C virus infections uncover molecular determinants for E2 targeting and vaccine design. *PLoS Pathog.* **15**, e1007772 (2019).
41. M. Law *et al*., Broadly neutralizing antibodies protect against hepatitis C virus quasispecies challenge. *Nat. Med.* **14**, 25–27 (2008).
42. Z. Y. Keck *et al*., Analysis of a highly flexible conformational immunogenic domain a in hepatitis C virus E2. *J. Virol.* **79**, 13199–13208 (2005).
43. Y. Li *et al*., Structural basis for penetration of the glycan shield of hepatitis C virus E2 glycoprotein by a broadly neutralizing human antibody. *J. Biol. Chem.* **290**, 10117–10125 (2015).
44. I. Vasiliauskaite *et al*., Conformational flexibility in the immunoglobulin-like domain of the hepatitis C virus glycoprotein E2. *MBio* **8**, e00382-17 (2017).
45. L. J. Ströh, K. Nagarathinam, T. Krey, Conformational flexibility in the CD81-binding site of the hepatitis C virus glycoprotein E2. *Front. Immunol.* **9**, 1396 (2018).
46. E. Giang *et al*., Human broadly neutralizing antibodies to the envelope glycoprotein complex of hepatitis C virus. *Proc. Natl. Acad. Sci. U.S.A.* **109**, 6205–6210 (2012).
47. F. Chen *et al*., Antibody responses to immunization with HCV envelope glycoproteins as a baseline for B-cell-based vaccine development. *Gastroenterology* **158**, 1058–1071.e6 (2020).
48. C. Fauvelle *et al*., Hepatitis C virus vaccine candidates inducing protective neutralizing antibodies. *Expert Rev. Vaccines* **15**, 1535–1544 (2016).
49. T. R. Fuerst, B. G. Pierce, Z. Y. Keck, S. K. H. Foung, Designing a B Cell-Based vaccine against a highly variable hepatitis C virus. *Front. Microbiol.* **8**, 2692 (2018).
50. H. Zazrin, H. Shaked, J. H. Chill, Architecture of the hepatitis C virus E1 glycoprotein transmembrane domain studied by NMR. *Biochim. Biophys. Acta* **1838**, 784–792 (2014).
51. L. Kong *et al*., Hepatitis C virus E2 envelope glycoprotein core structure. *Science* **342**, 1090–1094 (2013).
52. L. Kong *et al*., Structure of hepatitis C virus envelope glycoprotein E1 antigenic site 314-324 in complex with antibody IGH526. *J. Mol. Biol.* **427**, 2617–2628 (2015).
53. R. Spadaccini *et al*., Structural characterization of the transmembrane proximal region of the hepatitis C virus E1 glycoprotein. *Biochim. Biophys. Acta* **1798**, 344–353 (2010).
54. N. Tzarum *et al*., Genetic and structural insights into broad neutralization of hepatitis C virus by human VH1-69 antibodies. *Sci. Adv.* **5**, eaav1882 (2019).
55. J. S. McLellan *et al*., Structure-based design of a fusion glycoprotein vaccine for respiratory syncytial virus. *Science* **342**, 592–598 (2013).
56. R. W. Sanders *et al*., A next-generation cleaved, soluble HIV-1 Env trimer, BG505 SOSIP.664 gp140, expresses multiple epitopes for broadly neutralizing but not non-neutralizing antibodies. *PLoS Pathog.* **9**, e1003618 (2013).
57. H. M. Yassine *et al*., Hemagglutinin-stem nanoparticles generate heterosubtypic influenza protection. *Nat. Med.* **21**, 1065–1070 (2015).
58. L. Rutten *et al*., Structure-based design of prefusion-stabilized filovirus glycoprotein trimers. *Cell Rep.* **30**, 4540–4550.e3 (2020).
59. J. L. Slon-Campos *et al*., A protective Zika virus E-dimer-based subunit vaccine engineered to abrogate antibody-dependent enhancement of dengue infection. *Nat. Immunol.* **20**, 1291–1298 (2019).
60. B. S. Graham, M. S. A. Gilman, J. S. McLellan, Structure-based vaccine antigen design. *Annu. Rev. Med.* **70**, 91–104 (2019).
61. M. Kanekiyo, B. S. Graham, Next-generation influenza vaccines. *Cold Spring Harb. Perspect. Med.* a038448 (2020).
62. L. D. Jones, M. A. Moody, A. B. Thompson. Innovations in HIV-1 vaccine design. *Clin. Ther.* **42**, 499–514 (2020).
63. Y. Lu, J. P. Welsh, J. R. Swartz, Production and stabilization of the trimeric influenza hemagglutinin stem domain for potentially broadly protective influenza vaccines. *Proc. Natl. Acad. Sci. U.S.A.* **111**, 125–130 (2014).
64. E. Kim *et al*., Microneedle array delivered recombinant coronavirus vaccines: Immunogenicity and rapid translational development. *EBioMedicine* **55**, 102743 (2020).
65. W. Tai *et al*., A recombinant receptor-binding domain of MERS-CoV in trimeric form protects human dipeptidyl peptidase 4 (hDPP4) transgenic mice from MERS-CoV infection. *Virology* **499**, 375–382 (2016).
66. Y. C. Chang *et al*., Efficacy of heat-labile enterotoxin B subunit-adjuvanted parenteral porcine epidemic diarrhea virus trimeric spike subunit vaccine in piglets. *Appl. Microbiol. Biotechnol.* **102**, 7499–7507 (2018).
67. P. Leblanc *et al*., VaxCelerate II: Rapid development of a self-assembling vaccine for lassa fever. *Hum. Vaccin. Immunother.* **10**, 3022–3038 (2014).
68. T. B. Ruwona, E. Giang, T. Nieusma, M. Law, Fine mapping of murine antibody responses to immunization with a novel soluble form of hepatitis C virus envelope glycoprotein complex. *J. Virol.* **88**, 10459–10471 (2014).
69. W. Cai *et al*., Expression, purification and immunogenic characterization of hepatitis C virus recombinant E1E2 protein expressed by Pichia pastoris yeast. *Antiviral Res.* **88**, 80–85 (2010).
70. M. Logan *et al*., Native folding of a recombinant gpE1/gpE2 heterodimer vaccine antigen from a precursor protein fused with Fc IgG. *J. Virol.* **91**, e01552-16 (2016).
71. L. Cao *et al*., Functional expression and characterization of the envelope glycoprotein E1E2 heterodimer of hepatitis C virus. *PLoS Pathog.* **15**, e1007759 (2019).
72. B. Wen *et al*., Signal peptide replacements enhance expression and secretion of hepatitis C virus envelope glycoproteins. *Acta Biochim. Biophys. Sin. (Shanghai)* **43**, 96–102 (2011).
73. J. N. Glover, S. C. Harrison, Crystal structure of the heterodimeric bZIP transcription factor c-Fos-c-Jun bound to DNA. *Nature* **373**, 257–261 (1995).
74. B. E. Willcox *et al*., Production of soluble alphabeta T-cell receptor heterodimers suitable for biophysical analysis of ligand binding. *Protein Sci.* **8**, 2418–2423 (1999).
75. A. Berthelmann, J. Lach, M. A. Gräwert, M. Groll, J. Eichler, Versatile C(3)-symmetric scaffolds and their use for covalent stabilization of the foldon trimer. *Org. Biomol. Chem.* **12**, 2606–2614 (2014).
76. D. Wrapp *et al*., Cryo-EM structure of the 2019-nCoV spike in the prefusion conformation. *Science* **367**, 1260–1263 (2020).
77. S. E. Boyken *et al*., De novo design of protein homo-oligomers with modular hydrogen-bond network-mediated specificity. *Science* **352**, 680–687 (2016).
78. Z. Y. Keck *et al*., Human monoclonal antibody to hepatitis C virus E1 glycoprotein that blocks virus attachment and viral infectivity. *J. Virol.* **78**, 7257–7263 (2004).
79. T. J. Broering *et al*., Identification and characterization of broadly neutralizing human monoclonal antibodies directed against the E2 envelope glycoprotein of hepatitis C virus. *J. Virol.* **83**, 12473–12482 (2009).
80. R. E. Iacob, I. Perdivara, M. Przybylski, K. B. Tomer, Mass spectrometric characterization of glycosylation of hepatitis C virus E2 envelope glycoprotein reveals extended microheterogeneity of N-glycans. *J. Am. Soc. Mass Spectrom.* **19**, 428–444 (2008).
81. R. A. Urbanowicz *et al*., Antigenicity and immunogenicity of differentially glycosylated hepatitis C virus E2 envelope proteins expressed in mammalian and insect cells. *J. Virol.* **93**, e01403-18 (2019).
82. A. V. Gandhi, M. R. Pothecary, D. L. Bain, J. F. Carpenter, Some lessons learned from a comparison between sedimentation velocity analytical ultracentrifugation and size exclusion chromatography to characterize and quantify protein aggregates. *J. Pharm. Sci.* **106**, 2178–2186 (2017).

83. Z. Y. Keck *et al*., Human monoclonal antibodies to a novel cluster of conformational epitopes on HCV E2 with resistance to neutralization escape in a genotype 2a isolate. *PLoS Pathog.* **8**, e1002653 (2012).
84. Z. Y. Keck *et al*., Mapping a region of hepatitis C virus E2 that is responsible for escape from neutralizing antibodies and a core CD81-binding region that does not tolerate neutralization escape mutations. *J. Virol.* **85**, 10451–10463 (2011).
85. R. Gopal *et al*., Probing the antigenicity of hepatitis C virus envelope glycoprotein complex by high-throughput mutagenesis. *PLoS Pathog.* **13**, e1006735 (2017).
86. B. G. Pierce *et al*., Global mapping of antibody recognition of the hepatitis C virus E2 glycoprotein: Implications for vaccine design. *Proc. Natl. Acad. Sci. U.S.A.* **113**, E6946–E6954 (2016).
87. Y. Wang *et al*., Affinity maturation to improve human monoclonal antibody neutralization potency and breadth against hepatitis C virus. *J. Biol. Chem.* **286**, 44218–44233 (2011).
88. A. G. Khan *et al*., Structure of the core ectodomain of the hepatitis C virus envelope glycoprotein 2. *Nature* **509**, 381–384 (2014).
89. A. Wahid *et al*., Disulfide bonds in hepatitis C virus glycoprotein E1 control the assembly and entry functions of E2 glycoprotein. *J. Virol.* **87**, 1605–1617 (2013).
90. J. Dubuisson, C. M. Rice, Hepatitis C virus glycoprotein folding: Disulfide bond formation and association with calnexin. *J. Virol.* **70**, 778–786 (1996).
91. P. Angel, M. Karin, The role of Jun, Fos and the AP-1 complex in cell-proliferation and transformation. *Biochim. Biophys. Acta* **1072**, 129–157 (1991).
92. M. Karin, Zg. Liu, E. Zandi, AP-1 function and regulation. *Curr. Opin. Cell Biol.* **9**, 240–246 (1997).
93. K. A. Swanson *et al*., A respiratory syncytial virus (RSV) F protein nanoparticle vaccine focuses antibody responses to a conserved neutralization domain. *Sci. Immunol.* **5**, eaba6466 (2020).
94. J. Marcandalli *et al*., Induction of potent neutralizing antibody responses by a designed protein nanoparticle vaccine for respiratory syncytial virus. *Cell* **176**, 1420–1431.e17 (2019).
95. A. M. Owsianka *et al*., Identification of conserved residues in the E2 envelope glycoprotein of the hepatitis C virus that are critical for CD81 binding. *J. Virol.* **80**, 8695–8704 (2006).
96. K. McCaffrey *et al*., An optimized hepatitis C virus E2 glycoprotein core adopts a functional homodimer that efficiently blocks virus entry. *J. Virol.* **91**, e01668-16 (2017).
97. M. Q. Marín *et al*., Optimized hepatitis C virus (HCV) E2 glycoproteins and their immunogenicity in combination with MVA-HCV. *Vaccines (Basel)* **8**, E440 (2020).
98. E. H. Augestad *et al*., Global and local envelope protein dynamics of hepatitis C virus determine broad antibody sensitivity. *Sci. Adv.* **6**, eabb5938 (2020).
99. B. G. Pierce *et al*., Structure-based design of hepatitis C virus E2 glycoprotein improves serum binding and cross-neutralization. *J. Virol.* **94**, e00704-20 (2020).
100. Z. Keck *et al*., Cooperativity in virus neutralization by human monoclonal antibodies to two adjacent regions located at the amino terminus of hepatitis C virus E2 glycoprotein. *J. Virol.* **87**, 37–51 (2013).
101. Z. Y. Keck *et al*., Hepatitis C virus E2 has three immunogenic domains containing conformational epitopes with distinct properties and biological functions. *J. Virol.* **78**, 9224–9232 (2004).
102. Z. Y. Keck *et al*., Affinity maturation of a broadly neutralizing human monoclonal antibody that prevents acute hepatitis C virus infection in mice. *Hepatology* **64**, 1922–1933 (2016).
103. J. Lebowitz, M. S. Lewis, P. Schuck, Modern analytical ultracentrifugation in protein science: A tutorial review. *Protein Sci.* **11**, 2067–2079 (2002).
104. T. M. Laue, B. D. Shah, T. M. Ridgeway, S. L. Pelletier, *Analytical Ultracentrifugation in Biochemistry and Polymer Science* (Royal Society of Chemistry, 1992).
105. A. K. Andrianov *et al*., Supramolecular assembly of Toll-like receptor 7/8 agonist into multimeric water-soluble constructs enables superior immune stimulation in vitro and in vivo. *ACS Appl. Bio Mater.* **3**, 3187–3195 (2020).
106. A. K. Andrianov, Y. Y. Svirkin, M. P. LeGolvan, Synthesis and biologically relevant properties of polyphosphazene polyacids. *Biomacromolecules* **5**, 1999–2006 (2004).
107. A. K. Andrianov, A. Marin, T. R. Fuerst, Molecular-level interactions of polyphosphazene immunoadjuvants and their potential role in antigen presentation and cell stimulation. *Biomacromolecules* **17**, 3732–3742 (2016).
108. G. Wang, R. N. de Jong, E. T. J. van den Bremer, P. W. H. I. Parren, A. J. R. Heck, Enhancing accuracy in molecular weight determination of highly heterogeneously glycosylated proteins by native tandem mass spectrometry. *Anal. Chem.* **89**, 4793–4797 (2017).